Chemical Physics 77 (1983) 301–318
North-Holland Publishing Company

MONTE CARLO CALCULATIONS ON UNIMOLECULAR REACTIONS, ENERGY TRANSFER, AND IR-MULTIPHOTON DECOMPOSITION ‡

John R. BARKER

Department of Chemical Kinetics, SRI International Menlo Park California 94025, USA

Received 29 December 1982

Monte Carlo techniques are described for stochastic calculations involving energy transfer unimolecular reactions and IR-multiphoton decomposition, all of these phenomena can be simulated using the same computer code The details of the model are presented along with the following example calculations (1) weak collision energy-transfer following photoactivation (2) chemical activation unimolecular reactions with multiple reaction pathways, (3) incubation times in shock-tube experiments on systems with multiple reaction pathways, and (4) IR-multiphoton absorption and decomposition in collisional environments The model uses a modular approach that permits application to numerous experimental systems

1. Introduction

Information about highly vibrationally excited molecules (HVEMs) in the ground electronic state comes from experiments of many types, and calculations simulating the experiments are necessary for detailed interpretations Unimolecular reaction studies [1,2] that employ collisional activation, chemical activation, and photoactivation have been mostly concerned with the gross features of collisional energy transfer and the properties of the chemical reaction channels. Infrared laser multiphoton absorption (MPA) and decomposition (MPD) have been concerned with the spectroscopic properties of HVEMs and their unimolecular decomposition reactions [3,4] Other studies of HVEMs have employed photodecomposition of a precursor or unimolecular reactions to prepare HVEMs that are observed by infrared fluorescence [5,6]. Recently, photoactivation has been used to prepare HVEMs that have been studied using time-dependent thermal lensing [7] and infrared fluorescence [8–11]. Similarly, photoactivated isomerization reactions have been followed with time-resolved ultraviolet absorbance measurements [12] and by Raman-scattering techniques [13]. Other experiments have used overtone pumping to prepare HVEMs that can undergo unimolecular reactions [14,15] or emit in the infrared [16]. Results of most of these experiments are consistent with rapid intramolecular vibrational energy redistribution (IVR), but some experiments show effects that may be due to the finite rates of IVR [17]. For present purposes, IVR rates will be assumed to be very fast, so that isolated collisional systems behave microcanonically and only total energy is necessary to specify physical and chemical properties.

The Monte Carlo methods described in this paper are appropriate for describing many aspects of HVEMs and simulating experiments. Relatively simple versions of the theory have been employed, but extensions to more complex cases are often straightforward. The model includes the effects of collisional activation and deactivation, infrared laser MPA, simultaneous unimolecular reaction by several independent reaction channels, and infrared fluorescence by the HVEMs. Phenomena which can be readily treated using the model include fast thermal unimolecular reactions, chemical activation, photoactivation, energy transfer involving HVEMs, infrared MPA and MPD, and infrared fluorescence (IRF) from the HVEMS.

‡ Supported by the U S Department of Energy, Office of Basic Energy Sciences under Contract No DE-AM03-76-SF0115.

0301-0104/83/0000–0000/$03.00

This paper is intended to provide documentation of the methods we have been using to simulate our experimental data for several phenomena.

An advantage of Monte Carlo methods is that energy-graining is not necessary, and thus, it is easy to treat very large and very small energy steps in the same calculation. In addition, computer central processor memory space requirements are minimized and programming is relatively simple A drawback of Monte Carlo methods is that they tend to be time-consuming and, reliable calculations of "rare"events (i.e. events of low probability) require many trajectories, because precision is proportional to $N^{1/2}$, where N is the number of "trajectories". In our laboratory, this drawback is not a great handicap since we use a laboratory computer that costs little to operate.

In the next section, the Gillespie exact stochastic method (ESM) [18] is described. Models for each of the various physical and chemical processes are then outlined in some detail. In the final section, example calculations are presented, illustrating applications to several important physical phenomena.

2. Exact stochastic method

The dynamics of HVEMs can be described in terms of master equations in which the rate of change of population at energy E is equated to the sum of rates of production and loss of population. For practical computations, the continuous energy-space can be arbitrarily segmented into a finite number of "grains" and the energy-grained master equation (EGME) can then be solved by standard numerical techniques. For systems that possess significant fine structure, the energy graining must be sufficiently fine-grained so that accurate numerical results are obtained, and this often requires very large computer memory space.

Stochastic methods can be used to solve the same problems that are amenable to solution with EGMEs, and energy graining is not always necessary. Stochastic methods have the same relationship to solution of EGMEs as Monte Carlo integration has to conventional numerical integration. The exact stochastic method (ESM) developed by Gillespie [18] gives an exact solution to problems that can be formulated as master equations, and it is the method employed in our model calculations.

For the calculations presented here, we will assume complete stochasticity, in which a molecule loses all memory of its past history and the probabilities of subsequent potential fates do not depend on past history, but can only depend on the total energy of the molecule. For example, at any energy E, a molecule has a finite probability P_{c_i} of undergoing a collision (P_{c_i} is independent of E) with the ith collider gas, or it may react with probability $P_{r_j}(E)$ to form product species corresponding to reaction channel j. These probabilities are independent of the past history of the molecule, and they must sum to unity. The ESM is used to formulate the probabilities from the kinetic rates and rate constants that would be used in a master equation description of the process. Moreover, the ESM defines the time-increments of the calculation in a manner rigorously consistent with the probabilities and with the kinetic rate constants.

For a full description of the ESM, the lucid discussion [18] by Gillespie should be consulted. In an earlier paper, application of the ESM to collision-free IR-multiphoton decomposition was described [19]. For convenience, a brief outline adapted from Gillespie's discussion [18] is presented here.

Consider a molecule excited to energy E, which can undergo collisions, optical transitions, and unimolecular reactions. Several "reaction channels" are available to the molecule, including stimulated emission and absorption of photons, activating and deactivating collisions, and irreversible unimolecular reactions. Gillespie's approach is to define a joint probability density function that is the product of two terms: (1) the probability that a molecule, which arrives at state (energy) m at time t, will not undergo "reaction" during the next time interval τ; (2) the probability that the molecule will "react" to give state n in the infinitesimal time interval $(t+\tau) \rightarrow (t+\tau+\mathrm{d}t)$. This joint transition probability density function can be expressed in "conditioned" form as the product of three terms:

$$P_{nm}(\tau, t)\mathrm{d}\tau = P_{1m}(t)P_{2m}(\tau, t)\,\mathrm{d}\tau P_{3nm}(t, \tau), \quad (1)$$

where P_{1m} is the probability that the molecule will eventually leave state m; given that $P_{1m}(t) \neq 0$, $P_{2m}(\tau,t)\mathrm{d}\tau$ is the probability that the molecule, having arrived in state m at time t, will "react" during the interval $(\tau + t) \rightarrow (\tau + t + \mathrm{d}\tau)$; $P_{3nm}(t, \tau)$ is the probability that the "reaction" will produce state n, given that it "reacts" at time $t + \tau$. To express these probabilities, it is convenient to define $A_m(\tau) = \Sigma A_{nm}(\tau)$, the total probability density for "reaction" of molecules in state m. Then,

$$P_{1m}(t) = 1 - \exp[-B_m(\infty)], \quad (2)$$

where

$$B_m(\tau) = \int_0^\tau A_m(\tau')\mathrm{d}\tau', \quad (3a)$$

$$P_{2m}(\tau, t) = A_m(\tau)\exp[-B_m(\tau)]/\{1 - \exp[-B_m(\infty)]\}, \quad (3b)$$

$$P_{3nm}(\tau, t) = A_{nm}(\tau)/A_m(\tau). \quad (3c)$$

The procedure for simulating the random walk in energy space is to use two random numbers, r_1 and r_2 from the unit-interval distribution. For each collision, the time interval τ is chosen to that

$$\int_0^\tau A_m(\tau')\mathrm{d}\tau' = \ln(1/r_1), \quad (4)$$

assuming that $\ln(1/r_1) < \int_0^\infty A_m(\tau')\mathrm{d}\tau'$. If the inequality is not satisfied, $\tau = \infty$, and the random walk is terminated. The "reaction" channel n is chosen with another random number r_2 according to

$$\sum_{j=1}^{n-1} A_{jm}(\tau) < r_2 A_m(\tau) \leqslant \sum_{j=1}^{n} A_{jm}(\tau). \quad (5)$$

For random walks subject to $A_{nm}(\tau) =$ constant, the procedure is identical to that described previously [19]. For time-dependent $A_{nm}(\tau)$, the functional form for the time dependence must be known; if the integration in eq. (4) can be carried out in closed form, the procedure is facilitated. Gillespie gives several general examples, and specific examples are discussed below.

The procedure used in the present work is to calculate random walks (trajectories) for many individual molecules and retain a temporal record of the average values of important parameters, such as excitation energy, average number of photons absorbed, population distribution, temperature, etc. By averaging sufficiently large numbers of trajectories, suitable precision can be attained.

For rate processes that are independent of time ($A_m(t) = a_m$), integration of eq. (4) is straightforward and the time increment prior to the next collision is given by

$$\tau = (1/a_m)\ln(1/r_1) \quad (6)$$

When $A_m(t)$ is not constant, determination of the time interval is more difficult and may require solution of an integral equation. A simple example presented by Gillespie [18] is the case for $A_m(\tau) = a_m \exp(-k\tau)$. For a laser pulse that decays exponentially, the rates of photon absorption and stimulated emission are of exponential form. For this case,

$$\int_0^\tau A_m(t)\mathrm{d}t = (a/k)[1 - \exp(-k\tau)], \quad (7)$$

$$\tau = -(1/k)\ln[1 - (k/a_m)\ln(1/r_1)],$$

$$a_m/k > \ln(1/r_1).$$

A more general case, which must be treated routinely in the model calculations, applies when collisions can occur during a laser pulse with an exponential decay (other decay functions can be used) Under these conditions

$$A_m(t) = \omega t + \sigma(I_0/h\nu)\exp(-kt), \quad (8)$$

where ω is the collision frequency, σ is the optical absorption coefficient, I_0 is the initial laser intensity, $h\nu$ is the laser photon energy, and k is the decay rate of the laser pulse. Integrating eq. (8), we have

$$\omega\tau + \sigma(I_0/h\nu)\exp(-kt)[1 - \exp(-k\tau)] = \ln(1/r_1) \quad (9)$$

which must be solved for τ. The method used in our calculations is an iterative search where the first estimate is given by

$$\tau_0 = \frac{\ln(1/r_1)}{\omega + \sigma(I_0/h\nu)\exp(-kt)} \tag{10}$$

and subsequent estimates τ_i are calculated based on the previous estimates τ_{i-1}:

$$\tau_i = (1/\omega)\{\ln(1/r_1) - (\sigma I_0/h\nu)\exp(-kt)[1-\exp(-k\tau_{i-1})]\}. \tag{11}$$

This process is continued until τ_i has converged to within an error limit, typically 1%.

In summary, the procedure is to calculate many individual "trajectories" in energy space and average the results to get ensemble average behavior. During each trajectory, events take place at random intervals, which are selected using the Monte Carlo techniques described. On occurrence of each event, a decision is made concerning its fate, i.e. whether the event is a collision, optical transition, or chemical reaction. The decision is made according to a Monte Carlo technique Depending on the result of the decision, further decisions must be made, e.g if it is decided that a collision takes place, it must also be decided whether the collision represents activation or deactivation. The following sections describe the methodology for making such decisions.

3. Collisional transitions

For a full description of collisions, it is necessary to calculate the collision frequency ω_i involving the ith pair of distinguishable species and to know the transition probability functions $P_i(E, E')$. These functions describe the probability that a molecule initially possessing internal energy E will be found in the energy range E' to $E' + \mathrm{d}E'$ following a single collision. The product $\omega_i P_i(E, E')$ is the effective first-order rate constant for populating energy E' from molecules initially at energy E.

Most cases of interest involve pure substances or binary mixtures. The frequency of collisions between the molecule of interest, i, and the jth species of the mixture is given by [20]

$$\omega_{i,j} = N_j \pi \sigma_{ij}^2 \Omega_{ij}^{2,2} (8k_B T/\pi\mu_{ij})^{1/2}, \tag{12}$$

where N_j is the concentration of the jth species, σ_{ij} is the Lennard-Jones collision diameter for the pair of colliders, $\Omega_{ij}^{2,2}$ is the collision integral for the colliders, based on ϵ_{ij} (the Lennard-Jones well depth), k_B is the Boltzmann constant, T is the temperature, and μ_{ij} is the reduced mass for the collision pair. The collision integral can be approximated conveniently by [21]

$$\Omega_{ij}^{2,2} = [0.636 + 0\ 246 \ln(k_B T/\epsilon_{ij})]^{-1}. \tag{13}$$

The combining rules [20] used for deriving σ_{ij} and ϵ_{ij} from the Lennard-Jones parameters for the pure gases are

$$\sigma_{ij} = \tfrac{1}{2}(\sigma_{ii} + \sigma_{jj}), \quad \epsilon_{ij} = (\epsilon_{ii}\epsilon_{jj})^{1/2}. \tag{14}$$

Various forms for $P_i(E, E')$ have been proposed [1], but the experimental data on energy-transfer involving large molecules do not clearly point to a particular choice. There are indications, however, that the "exponential" model, in which small energy steps dominate, is appropriate for inefficient colliders, while the "stepladder" or "Gaussian" models, in which large energy steps dominate, are appropriate for more efficient colliders. Whatever model is used, Monte Carlo techniques can be employed to select the energy step in a given collision, and the more numerically tractable functions for $P_i(E, E')$ are more computationally efficient.

For our calculations, we have used two arbitrary models for $P_i(E, E')$. For *inefficient colliders*, the exponential model is used for down-steps:

$$P_{\mathrm{d},i}^{\mathrm{e}}(E, E') = \frac{\exp[-(E-E')/\alpha_{\mathrm{e}}]}{N(E)}, \quad E' < E. \tag{15}$$

For up-steps, microscopic reversibility is used to obtain,

$$P_{\mathrm{u},i}^{\mathrm{e}}(E, E') = \frac{\rho(E')}{\rho(E)} \frac{\exp[-(E'-E)/\alpha_{\mathrm{e}}]}{N(E')} \times \exp[-(E'-E)/k_B T], \quad E' > E, \tag{16}$$

where $\rho(E)$ is the density of vibrational states at energy E. In both of these expressions, α_e is equal to the average energy lost on a down-step. Since α_e may depend on E, we have incorporated a linear dependence, $\alpha = \beta + \gamma E$, although other functions may well be found to be more appropriate. The normalization factors $N(E)$ and $N(E')$ are not equal to one another, in general, and this difference becomes very important at low energies At high energies, $N(E) \approx N(E')$, and this approximation is suitable for unimolecular reaction calculations [22] The normalization factor is given by

$$N(E) = -\int_0^E P_{d,t}(E, x)\mathrm{d}x + \int_E^\infty P_{u,t}(E, x)\mathrm{d}x = C_d(E) + C_u(T, E), \quad (17)$$

where the down-steps and up-steps have been explicitly written. Since $N(E)$ and $N(E')$ are factors in the expression for $P_t(E, E')$, a proper evaluation of $N(E)$ requires solution of an integral equation at every energy E. Finite difference methods have been used for this purpose [23]. In the present work, an upper energy bound E_{max} is specified for the computations at an energy high enough so that $N(E) \approx N(E')$, and an approximate value of $N(E)$ is then calculated. This process is repeated at two slightly lower energies, and the calculated values of $N(E)$ are then used to predict $N(E)$ at still lower energies (quadratic extrapolation). Using this "bootstrap" method, $N(E)$ is calculated at any energy less than E_{max} with sufficient accuracy (if it is assumed that $N(E) \approx N(E')$ at all energies, the results are very similar, except at low energies).

The exponential model is appropriate for inefficient collisions, and emphasizes small step sizes. For more *efficient collisions*, we have employed the "reverse exponential" model, which emphasizes larger step sizes. For down steps

$$P^r_{d,t}(E, E') = \frac{\exp(-Z)}{N(E)} \times \{1 - \exp[-2(E' - E)/\alpha_r]\}, \quad (18)$$

$$\{\tfrac{1}{2}Z\alpha_r\} < E' < E.$$

For our calculations, we have chosen $Z = 3$. Detailed balance is invoked to obtain an expression for the up-steps. Again, calculation of $N(E)$ requires solution of an integral equation, and the approximate method previously outlined was employed. A major virtue of the "reverse exponential" model is its simplicity, but the abrupt discontinuities at the upper and lower extremes of energy are clearly unrealistic Examples of the exponential and reverse exponential modes are presented in fig. 1.

The Monte Carlo method used to select an energy step size requires two random numbers r_3 and r_4. First, the probability of an up-step is calculated·

$$P_{up}(T, E) = C_u(T, E)/N(E). \quad (19)$$

Then, random number r_3 is compared to $P_{up}(T, E)$: $r_3 > P_{up}(T, E)$ results in a down-step, and $r_3 < P_{up}(T, E)$ results in an up-step. In practice, evaluation of $P_{up}(T, E)$ at every time-step is not computationally efficient. The calculation is facilitated by calculating $P_{up}(T, E)$ at 100 equally spaced energies from zero to E_{max} and then, during the calculation, quadratic interpolation is per-

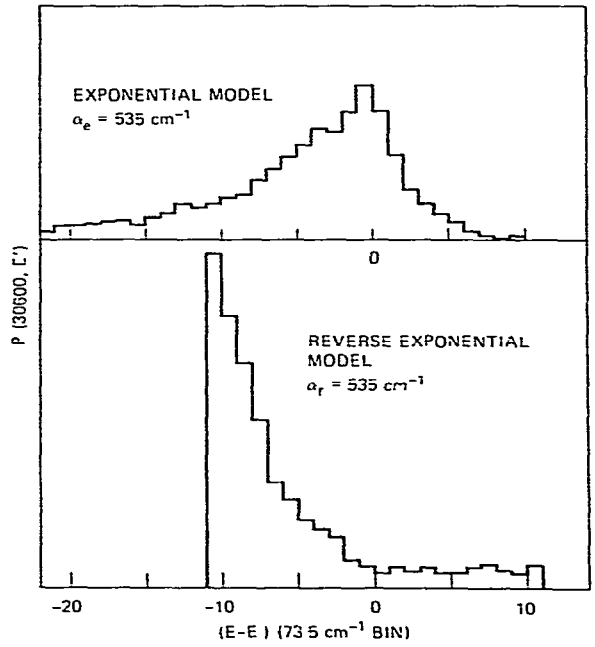

Fig 1 Examples of the exponential and reverse exponential models based on azulene collisions

formed to determine $P_{up}(T, E)$ Examples of the functional behavior of $P_{up}(T, E)$ are presented in fig. 2.

The calculation of energy-step magnitude depends on whether random number r_3 has selected an up-step or a down-step. For down-steps, the step size is calculated from the following equality:

$$r_4 = \int_E^E P_i(E, x)\mathrm{d}x \left[\int_0^E P_i(E, x)\mathrm{d}x\right]^{-1}. \quad (20)$$

For the chosen models, analytic functions can be derived:

$$(E - E')_c = -\alpha_c \ln\{1 - r_4[1 - \exp(-E/\alpha_c)]\}, \quad (21)$$

$$(E - E')_r = \alpha_r \ln\{1 - r_4[1 - \exp(-Z)]\}. \quad (22)$$

Calculation of up-step magnitudes is carried out using the expression

$$r_4 = \int_E^{E'} P_i(E, x)\mathrm{d}x \left[\int_E^{\infty} P_i(E, x)\mathrm{d}x\right]^{-1}. \quad (23)$$

Unfortunately, there are no simple analytic forms for this expression, and we have used a simple approximation that seems adequate for energies greater than the average thermal energy of the system Basically, the approach used is to assume that $N(E)$ is approximately independent of energy, and the ratio of densities of states can be approximated by

$$\rho(E')/\rho(E) = \exp[B(E' - E)]. \quad (24)$$

Using these approximations, the probability distribution for up-steps can be written

$$P_{u,}(E, E') \approx [1/N(E)]P_{d,}(E', E) \times \exp[(E' - E)(B - 1/k_B T)]. \quad (25)$$

For the two models used, this leads to integrated forms·

Exponential up-step

$$(E' - E)_e = -\frac{\ln r_4}{1/k_B T + 1/\alpha_e - B}. \quad (26)$$

Reverse exponential up-step

$$(E' - E)_r = \ln[r_4 \exp(E_f\delta) - 1) + 1]/\delta, \quad (27)$$

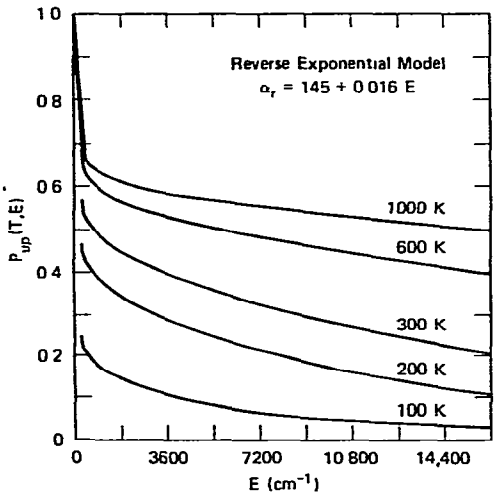

Fig 2 Probability of azulene collisional up-transition for various bath temperatures, showing variation with excited molecule internal energies

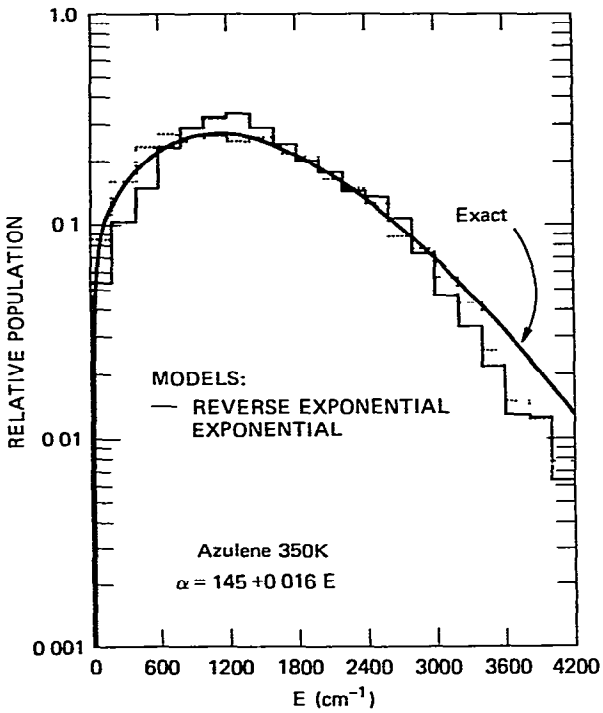

Fig 3. Thermal vibrational population distribution of azulene at 350 K. "Exact" is based on Whitten–Rabinovitch density of vibrational states

where

$$\delta = B + 1/\alpha_r - 1/k_B T,$$

and

$$E_\ell = (E + Z\beta)/(1 - Z\gamma) \quad \text{for } \alpha_r = \beta + \gamma E.$$

Because $\rho(E')/\rho(E)$ is not described exactly by eq. (24), the exponential model up-steps are over-estimated when $B > (1/k_B T + 1/\alpha_e)$. In such cases, B is set equal to $0.5(1/k_B T + 1/\alpha_e)$, in order to limit the large over-estimates of up-step size. Although arbitrary, this procedure seems to be effective since, for thermal collisions, the thermal vibrational energy content $\langle E_v(T)\rangle$ predicted by the model closely approximates that calculated using statistical mechanics and the Whitten–Rabinovitch vibrational state density, as illustrated in fig 3. The reverse exponential model up-steps are well approximated by eq. (27); furthermore, the maximum up-step size is automatically limited.

4. Temperature changes due to collision

In the Monte Carlo model presented here, the approach is to consider a single molecule (i.e. its vibrational energy) immersed in an inert heat-bath that can be a binary mixture of gases. When vibrational energy is lost from the single molecule, the heat-bath must get warmer, and when thermal energy from the bath is lost to give vibrational excitation in the single molecule, the bath must get cooler. Because the "activated" molecule is supposed to be representative of all other activated molecules, the temperature change of the heat bath is assumed to be given by:

$$\Delta T = (E' - E) N^* \left[\sum C_{V,i} N_i\right]^{-1}, \qquad (28)$$

where N^* is the concentration of "activated" molecules, $(E' - E)$ is the collision energy-step experienced by the single representative molecule, N_i is the concentration of the ith mixture component, and C_{V_i} is its heat capacity at constant volume (since C_{V_i} changes with temperature, a linear function for $C_{V_i}(T)$ is used in the calculation). The change in temperature modifies the bath temperature at every time-step, and the calculated value for collision frequency is also modified.

As the temperature changes, the collisional energy-step size distribution must also change appropriately. For the purpose of computational speed, $P_{up}(T, E)$ is calculated for T_0, the initial temperature prior to starting trajectories An approximate correction is applied during the trajectories to account for temperature changes·

$$P_{up}(T, E) = \frac{(T/T_0) P_{up}(T_0, E)}{1 + (T/T_0 - 1) P_{up}(T_0, E)}. \qquad (29)$$

This form is rigorously correct as long as the ratio $N(E)/N(E')$ is independent of T and it is based on the fact that only $C_u(T, E)$ depends on temperature. For temperature changes as great as a factor of two, it is an adequate approximation, as may be determined from the functions presented in fig. 4.

Because the Monte Carlo selection of collision-step sizes can result in large steps, the temperature excursions can be quite large if the mole fraction of activated molecules is large. Because the single molecule is not necessarily a realistic representative of the average activated molecule, unrealistic temperature and energy excursions will occur in the calculation. There are compensating factors, however, that tend to reduce the effect of large excursions Given a large up-step, for example, the

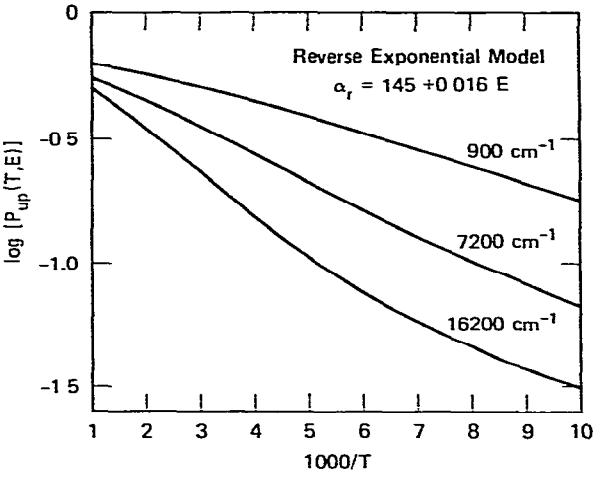

Fig 4 Probability of a collisional up-transition for various excited azulene internal energies, showing variation with temperature [from eq. (16)]

bath temperature falls, and the probability of an up-step on the next collision is lowered (the collision frequency is also reduced slightly). Thus, an unusually large energy-step is ameliorated in subsequent steps, and although the model is not realistic in allowing the single molecule to represent the entire population of activated molecules, the calculated results appear to be reasonable in this regard For small mole fractions of activated molecules, the temperature excursions are very small and do not affect the calculated results.

5. Optical transitions

The master equation for infrared multiple photon absorption and application of the ESM to its solution have been described elsewhere [19,24], but a brief description is included here for completeness The effective first-order rate constants for absorption (C_i^a), and stimulated emission (C_i^e) are assumed to be linearly dependent on the laser intensity $I(\lambda)$ (i e. incoherent single-photon transitions):

$$C_i^a = \sigma(\lambda, E_i) I(\lambda)/\epsilon_\ell,$$
$$C_i^e/C_i^a = g(E_i)/g(E_{i+1}) = \rho(E_i)/\rho(E_{i+1}), \quad (30)$$

where $\sigma(\lambda, E_i)$ is the absorption coefficient of a molecule with energy E_i, λ is the wavelength of laser light of photon energy ϵ_ℓ, $g(E)$ is the degeneracy of states of energy E and $\rho(E)$ is the corresponding density of states. The functional form of $\sigma(\lambda, E_i)$ is, as yet, poorly understood, but there is some justification for a function of the form

$$\sigma(\lambda, E_i) = \sigma_0(\lambda)(1 + E_i/\epsilon_\ell)^{n(\lambda)}, \quad (31)$$

where $\sigma_0(\lambda)$ is the absorption coefficient for light of wavelength λ when the molecule is initially in its ground state; $n(\lambda)$ is a parameter that is expected to fall within the range $-1 < n(\lambda) < 1$. A generalized form of eq. (1) can take into account the thermal energy E_t that may reside in the molecule when $\sigma_0(\lambda)$ is measured·

$$\sigma(\lambda, E_i) = \sigma_0(\lambda)\left[(E_i + \epsilon_\ell)/(\epsilon_\ell + E_t)\right]^{n(\lambda)}. \quad (32)$$

These forms for rate coefficients and absorption coefficients are convenient and may be realistic for some molecules, but more sophisticated general models are being developed in other laboratories [25,26], and it is our intention to incorporate the more sophisticated models for optical transitions into future calculations.

6. Unimolecular reaction rate constants

Specific reaction rate constants $k(E)$ are needed for the calculation of unimolecular reaction rates; bimolecular reactions could also be treated in an analogous fashion. The theory of choice for calculating $k(E)$ is the RRKM theory [1,27,28], and RRKM rate constants can be incorporated in the model by interpolating between elements of an array containing exact numerical values. For many purposes, however, it is more convenient to use approximate expressions where the parameters have been adjusted to give close agreement with RRKM values for $k(E)$. From quantum RRK theory [19,27,28], the QRKK specific rate constant is given by

$$k(E) = A\frac{\Gamma(a+1)\Gamma(a-b+s)}{\Gamma(a-b+1)\Gamma(a+s)}, \quad (33)$$

where s is the number of oscillators, A is the pre-exponential factor of the high-pressure thermal unimolecular rate constant, and a and b are the reduced internal energy and reduced reaction critical energy, respectively.

$$a = E/h\langle\nu\rangle, \quad b = E_{crit}/h\langle\nu\rangle, \quad (34)$$

where $\langle\nu\rangle$ is the geometric mean vibrational frequency of the molecule. By treating A and E_{crit} as adjustable parameters, the QRRK expression can be used to fit RRKM rate constants, as shown in fig 5.

Another simple expression for $k(E)$, is given by the Laplace transform inversion of the Arrhenius form of the thermal unimolecular rate constant [29]. This expression is written

$$k(E) = A\rho(E - E_{crit})/\rho(E), \quad (35)$$

where A and E_{crit} may be used as adjustable parameters to closely approximate RRKM rate constants, as shown in fig. 5.

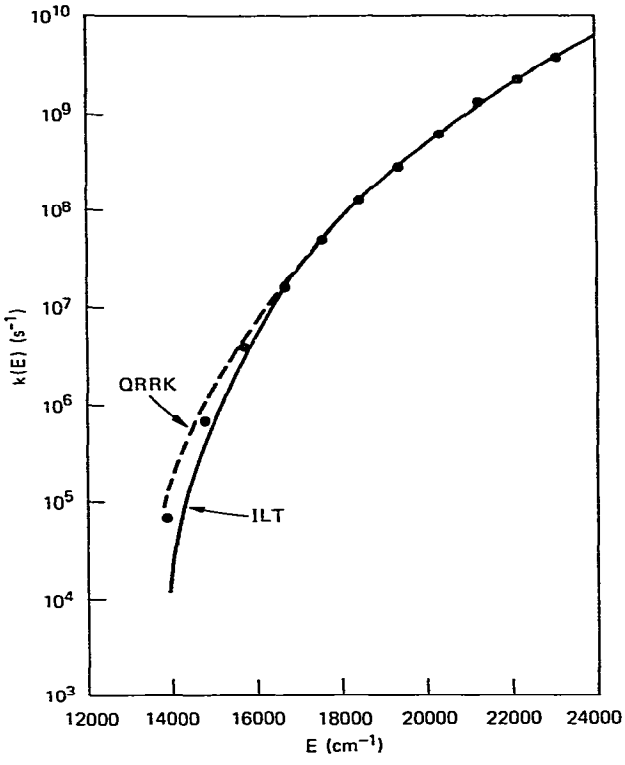

Fig 5. Unimolecular rate constants as a function of internal energy, calculated according to quantum RRK (QRRK) theory RRKM theory (solid points), and the approximate inverse Laplace transform (ILT) version of RRKM theory

Since most molecules possess numerous unimolecular reaction paths that differ in A and E_{crit}, we have incorporated up to three unimolecular reaction paths in the calculation. Additional unimolecular reaction channels can be included if desired.

Although RRKM theory is very useful, other approaches have been used with success. The adiabatic channel theory of Quack and Troe [30] has been applied to the decomposition of small molecules; angular momentum effects are treated explicitly in this approach. Minimum density of states models are also useful [31]. A recent Monte Carlo calculation by Stace and co-workers [32] used a different approach, but treated rotations explicitly, as did Holmlid and Rynefors [33]. Future development of the present model could incorporate a more sophisticated approach.

7. Infrared fluorescence

In a series of experiments [8–11] probing the energy-transfer dynamics of highly vibrationally excited molecules (HVEMs), we have used the infrared fluorescence (IRF) emitted by the ensemble of excited molecules to monitor their internal energy. This is a valuable technique that will be used more widely in the future. To perform model simulations of the data, it is necessary to predict the IRF emission intensity at a particular wavelength as a function of internal energy.

For a given vibrational fundamental of a single molecule, the emission intensity is given by [5,34]

$$I_{v,v-1} = h\nu_{v,v-1} A^{v,v-1} P_v. \tag{36}$$

where P_v is the population of level v, $\nu_{v,v-1}$ is the frequency of the transition, and $A^{v,v-1}$ is the Einstein coefficient for spontaneous emission. For at least the first few levels, the Einstein coefficients can be estimated by the harmonic oscillator approximation:

$$A^{v,v-1} \approx vA^{1,0} \tag{37}$$

For a molecule with total vibrational energy E distributed statistically,

$$P_v = [\rho_r(E - vh\nu)/\rho(E)]N, \tag{38}$$

where N is the total number density of the emitting species, $\nu = \nu_{v,v-1}$ (approximately the same for all v), $\rho(E)$ is the total density of vibrational states for all s modes, and $\rho_r(E - vh\nu)$ is the density of states of the $s-1$ modes, omitting the emitting mode and the energy residing in it. The total emission intensity is given by

$$I = \sum_{v=1}^{v_{max}} I_{v,v-1}, \tag{39}$$

where v_{max} is the maximum quantum number consistent with total vibrational energy E. If several different vibrational modes emit in the same wavelength band, the IRF intensity of the unresolved band is given by

$$I_T(E) = \sum_i I_i$$

$$I_T = \sum_i \sum_{v_i} v_i A_i^{1,0} \frac{\rho_{r,i}(E - v_i h\nu_i)}{\rho(E)} N h\nu_{v,v-1}. \tag{40}$$

This expression has been shown to be consistent with thermal emission intensities [5] and with the IRF from the C–H modes of azulene excited to selected energies [9]. Note that eq. (37) is not appropriate for overtone bands and combination bands, and other expressions for I must be employed.

When the calculations are performed, the IRF intensity is computed for 100 equally spaced energies from $E = 0$ to E_{max} prior to computing any trajectories As the trajectories are computed, values of IRF intensity at any energy are obtained by quadratic interpolation, a procedure that is far more rapid than calculating I_T at each separate energy sampled in the random walk.

8. Bookkeeping

Although the ESM as employed here has no intrinsic energy or time "graining", and thus can accurately perform computations on systems with large and small characteristic energy and time steps, "binning" must be employed in order to record intermediate values of the stochastic variables. For example, the time axis can be divided arbitrarily into a number of bins to record intermediate values of temperature, IRF, reaction yield, etc. "Bookkeeping" is the detailed process of binning and recording averages of intermediate values. Three bookkeeping subroutines are incorporated into the computer program:

A. All collisional transitions are categorized as "up" and "down" and are binned as a function of step-size. This permits inspection of the energy-transfer step-size distribution function.

B At the beginning of each time step, values of E, T, IRF, and the net number of photons absorbed are binned as a function of time. This permits reconstruction of average values of these variables and of population distributions for the time-history of the calculation.

C. When reaction occurs, the reaction channel is recorded, and the reaction time is binned. In addition, the internal energy of reacting molecules is binned. For MPD calculations, the logarithms of decomposition times are averaged to obtain the log-normal parameters [19,24] when appropriate.

Routine "A" is not strictly necessary, although convenient; "B" and "C" are necessary for most simulations. Since there are many parameters that are of interest and many techniques for bookkeeping may be employed, no further details will be presented here.

9. Representative example calculations

The examples included here are intended to illustrate applications of the model to various phenomena. *The examples are not accurate simulations of experimental data!* In our laboratory, the model has been used to treat energy transfer, MPA, MPD, and chemical activation, and this paper provides documentation of the method used, but the original papers should be consulted for simulations of actual experimental results.

9.1. Energy transfer

In a series of experiments employing photoactivation [8–11], collisional deactivation of highly excited azulene was monitored by IRF from the C–H stretch modes emitting near 3000 cm^{-1}. Typically, the azulene was initially at room temperature at a partial pressure of a few mTorr and intimately mixed with a collider gas, such as argon. Excitation of the azulene was achieved with a tunable dye laser or a nitrogen laser, and the experiments exploit the advantageous photophysical properties of azulene to give ensembles of HVEMs with a narrow distribution of initial energies.

The vibrational frequencies of azulene are used in the density of states calculation and in computing the IRF intensity. The thermal vibrational energy content is calculated in the harmonic oscillator approximation. The initial excitation energy is set equal to the laser photon energy added to the thermal vibrational energy content. The calculation parameters are presented in table 1.

The calculated IRF intensity versus time for an assumed value of α_e is presented in fig. 6, and the

Table 1
Molecular parameters

Molecule	C_v (cal K^{-1} $mole^{-1}$)	E_t (cm^{-1})	Lennard-Jones parameters		Whitten–Rabinovitch parameters		
			σ(Å)	ϵ/K	E_z (cm^{-1})	$\langle h\nu \rangle$ (cm^{-1})	β_{WR}
azulene	28 9	979	7 68	590	30892	1032.3	1.418
H_2O_4	16 6	604	4 55	577	6450 5	655 8	1 745
n—C_3H_7I	42 6	614	6 0	300	20360	1108 9	1 399
1,1,2-$C_2F_3H_3$	16 3	496	5.28	323	11479	970 5	1.377
Ar	3 0	–	3 542	93.3	–	–	–
N_2	5 0	–	3 798	71.4	–	–	–
CO_2	5 0	–	3 941	195 2	–	–	–

corresponding effective first-order rate constant may be compared to that determined from experiment. By comparisons such as this, the energy-transfer parameter for the various collider gases can be determined (see table 2).

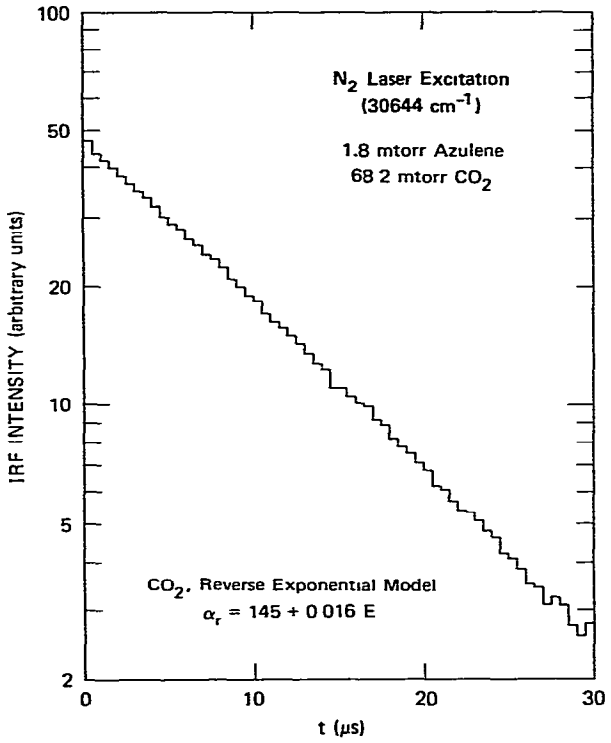

Fig 6. Decay of IRF intensity ($\lambda = 3\,3$ μm) due to the deactivation of excited azulene by CO_2.

Table 2
Energy-transfer parameter. $\alpha = \beta + \gamma E$

Collision pair	Model	β	γ
azulene + azulene	reverse exponential	95	0.0535
azulene + CO_2	reverse exponential	145	0.016
H_2O_4 + N_2	exponential	0	0 014
n-C_3H_7I + CO_2	reverse exponential	145	0 016
1,1,2-$C_2F_3H_3$ + Ar	exponential	50	0 01

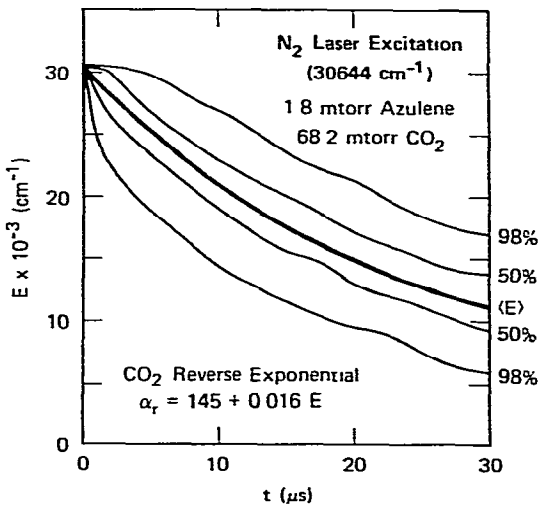

Fig 7 History of average internal energy and spread of population distribution corresponding to the azulene IRF decay shown in fig 6 Half of the total population lies between the lines labled "50%", and 98% of the population lies between the lines labled "98%".

Other information also results from the calculation, such as temporal histories of E, T, and population distribution. The temperature-history can be used in interpreting experiments using the time-dependent-thermal-lensing (TDTL) technique [7]. The ensemble average energy $\langle E(t) \rangle$ and an indication of the population distribution are presented in fig 7. These variables are directly related to absorption coefficients of the excited molecules (UV absorption has been used to follow energy transfer involving excited toluene prepared by photoisomerization of 1,3-cycloheptatriene [12]).

9.2. *Chemical activation – multiple reaction channels*

Calculational methods for treating chemical activation problems have been in use for many years; in fact, stochastic methods were among the first to be applied to such problems [35]. The ESM applied here is similar to earlier approaches in some respects, but the random time interval selection method developed by Gillespie is unique, and Monte Carlo methods for selection of collision step-size and reaction channel have rarely been employed.

The example calculation selected to illustrate application to multiple channel reactions is important in atmospheric chemistry. the self-reaction between two HO_2 free radicals (for recent references and experimental results, see refs. [36–38]). It has been conjectured that the reaction mechanism is as follows:

$$HO_2 + HO_2 \rightarrow H_2O_4(E), \qquad \text{(a)}$$

$$H_2O_4(E) \rightarrow HO_2 + HO_2, \qquad (-\text{a})$$

$$H_2O_4(E) \rightarrow H_2O_2 + O_2, \qquad \text{(b)}$$

$$H_2O_4(E) + N_2 \rightarrow H_2O_4(E') + N_2. \qquad \text{(c)}$$

The two unimolecular reaction channels available to $H_2O_4(E)$ at internal energy E are reactions $(-a)$ and (b). Partial de-excitation of $H_2O_4(E)$ by collision can also take place, and energy-transfer parameters must be assigned to process (c).

The parameters chosen for the example calculations are presented in the tables, and details concerning their selection can be found elsewhere

An important feature of chemical activation is the initial energy distribution of excited molecules formed by reaction (a). The correct distribution function [27,28] is derived from microscopic reversibility and the reverse reaction $(-a)$ This function could be incorporated in our model, but for present purposes, we have approximated the full distribution function by a delta function located at energy E [28, p. 214]:

$$E = E_{-a} + E_t(H_2O_4),$$

Table 3
Reaction parameters [a]

System	Reaction	Rate constant
H_2O_4	$HO_2 + HO_2 \xrightarrow{a} H_2O_4$	$k_{a\infty} = 1 \times 10^{-11}$ cm^3 s^{-1}
	$H_2O_4 \xrightarrow{-a} HO_2 + HO_2$	$\log k_{-a\infty} = 16\,05 - 9000/\theta$
	$\xrightarrow{b} H_2O_2 + O_2$	$\log k_{b\infty} = 11.9 - 6500/\theta$
n-C_3H_7I	n-$C_3H_7I \xrightarrow{d} C_3H_6 + HI$	$\log k_{d\infty} = 12\,9 - 16614/\theta$
	$\xrightarrow{e}$ n-$C_3H_7 + I$	$\log k_{e\infty} = 15\,5 - 18188/\theta$
1,1,2-$C_2F_3H_3$	1,1,2-$C_2F_3H_3 \xrightarrow{f} CH_2CF_2 + HF$	$\log k_{f\infty} = 12\,53 - 23714/\theta$
	$\xrightarrow{g}$ CHFCHF + HF	$\log k_{g\infty} = 13.23 - 23714/\theta$
	$\xrightarrow{h}$ CFH-CHF + HF	$\log k_{h\infty} = 13\,21 - 24413/\theta$

[a] $\theta = 2\,303\,RT$ in units of cm^{-1}

where E_{-a} is the critical energy for reaction (−a) and $E_t(H_2O_4)$ is the thermal vibrational energy content of H_2O_4 at the temperature of the experiment. This approximation is effective for illustrating the major features of the model, but is probably inadequate for explaining some of the finer details of pressure and temperature dependence.

To use the model for this calculation, a value of k_a (table 3) is obtained from other calculations [39] or is estimated, and $H_2O_4(E)$ is assumed to be formed. The result of the calculation is in the form of the probability P_t that $H_2O_4(E)$ will react according to channels (−a) or (b), or will be collisionally stabilized to form H_2O_4 in thermal equilibrium with the argon bath gas. As the pressure and temperature are varied, the relative probabilities change accordingly. The overall rate constant for formation of products is given by $k_p = k_a(1 + P_{-a})$ and k_p is shown as a function of pressure in fig 8, and as a function of temperature in fig. 9. A full discussion of these and other results will be presented elsewhere [40].

9.3. Incubation times – multiple channel reactions

In shock-tube experiments, the bath gas is heated very rapidly to a high temperature and a finite amount of time is necessary for reactant gases to reach a new equilibrium The time necessary is dependent on energy transfer. Once the reactant gas has been collisionally activated, its reaction rate constants (which are strongly temperature dependent) may have increased many-fold. If the rate of reaction is monitored as a function of time, the lag-time that is necessary for collisional activation of the reactants can be observed, and it is called the incubation time. The physical and chemical processes involved in the incubation period can be modelled conveniently using stochastic methods, although other methods have also been used [41].

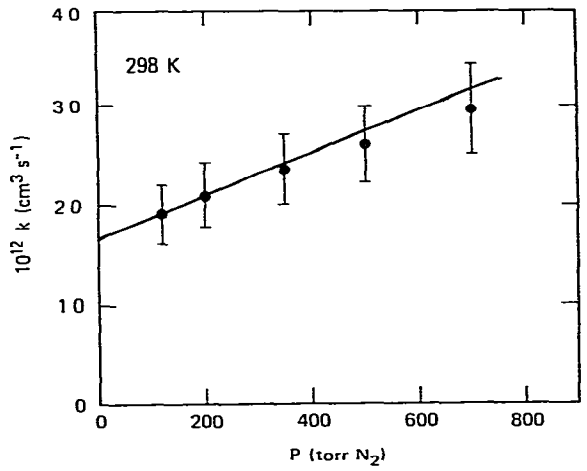

Fig 8 Global rate constant for loss of HO_2 radicals as a function of pressure

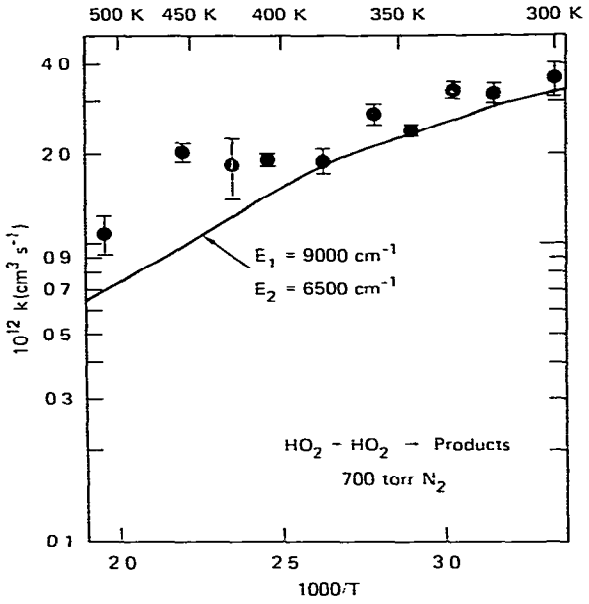

Fig 9 Global rate constant for loss of HO_2 radicals as a function of temperature (700 Torr N_2) Data points taken from ref [37]

For the purposes of illustration, the decomposition of *n*-propyl iodide was chosen. This reaction can proceed by two low-energy reaction pathways:

$$n\text{-}C_3H_7I \rightarrow HI + C_3H_6, \quad \text{(d)}$$

$$\rightarrow I + n\text{-}C_3H_7. \quad \text{(e)}$$

The branching ratio depends on the energy-transfer parameters, the pressure, and the temperature; each of these is treated in a self-consistent fashion by the model. This type of reaction may be important in the pyrolysis of fuel molecules in com-

bustion and shows what can occur with bimolecular reactions (in the pseudo-first-order limit), as well.

For present purposes, the RRKM parameters for *n*-propyl iodide decomposition were taken from the work of King et al. [42] and are presented in table 3. Calculations were carried out for the reverse exponential model. The calculations correspond to a shock-tube experiment at 2000 K and 3000 Torr pressure of CO_2. The results are presented in fig. 10, where the significant delay prior to the onset of decomposition is a manifestation of the incubation time. Changes of collision models and α values affect the incubation time. The reaction-branching ratio is also profoundly dependent upon collision model and α, as noted by several authors [1,43]. Thus, the experimental measurement of branching-ratio pressure-dependence is an important method for investigating some of the details of collisional energy transfer.

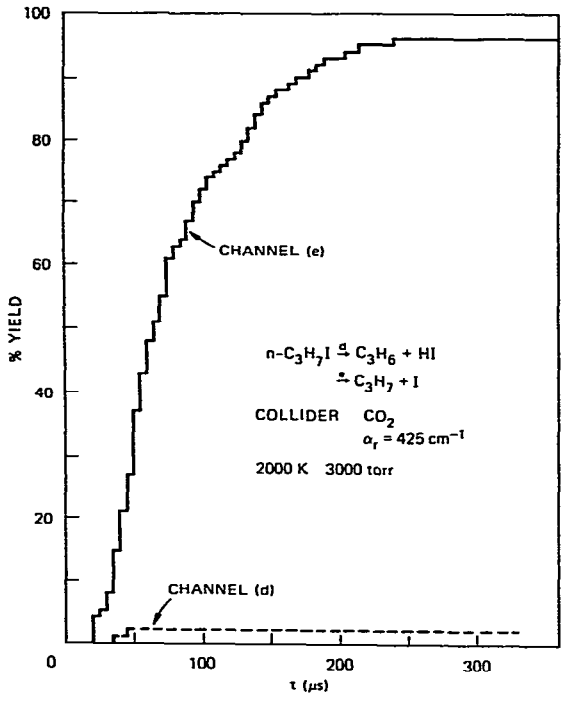

Fig 10 Incubation time and reaction branching ratio for a shock tube experiment simulation

9.4. Infrared multiple photon absorption and decomposition in collisional environments

In experiments that include infrared multiple photon excitation along with collisions, the internal energy of the subject molecule can change by relatively large amounts (e.g. 1000 cm^{-1}) due to photon absorption, or by very small amounts due to collisions It is in simulating experiments such as these that the Monte Carlo approach is most appropriate. If an energy-grained master equation is employed, the grain size must be small to properly simulate the collisions (especially when there are several reaction channels) and many grains are necessary to describe the system from $E = 0$ up to the maximum energy of the calculations. Furthermore, photon absorption terms, as well as collisional terms, must be included in the EGME. In a typical case, the value for α might be 250 cm^{-1} and the calculation maximum energy might be 50 000 cm^{-1}. To describe the collisions adequately may require a grain size of 25 cm^{-1}, resulting in 2000 energy levels whose populations must be calculated. Such calculations require a large computer memory and sophisticated numerical techniques [44–46]. Moreover, for multiple channel reactions, smaller grains may be necessary, and the calculations must be repeated several times to ensure that the solution has properly converged and is not sensitive to grain size.

The Monte Carlo techniques described in this paper do not require energy graining, eliminating a feature that is non-physical for the quasi-continuum. The absence of energy graining eliminates the necessity for large computer core, and it simplifies programming, making feasible large computations on small computers When large temperatures excursions occur, the Monte Carlo approach described here may be somewhat less accurate then the energy-grained master equation approach, due to the approximations involved, but more sophisticated approximations can be derived to improve accuracy.

In this context, it should be noted that an exponential decay of the laser pulse intensity was assumed in writing eq. (8). This assumption is not strictly necessary and, in other calculations we have even simulated a mode-locked laser pulse-

train by assuming a rapidly oscillating sine-wave bounded by a pulse envelope that rose and decayed according to the sum of two exponentials. For simulations of experiments in which the collision frequency is less than the decay constant of the laser pulse, almost any function is adequate. For more accurate simulations at higher pressures, however, more accurate representations of the laser pulse are necessary.

For an example of infrared laser-induced decomposition under collisional conditions, consider the reactions of 1,1,2-trifluoroethane. This molecule has several pathways for HF molecular elimination:

$$CF_2H\text{–}CFH_2 \xrightarrow{f} CH_2{=}CF_2 + HF,$$

$$\xrightarrow{g} CFH{=}CFH \text{ (cis and trans)} + HF,$$

$$\xrightarrow{h} CH_2FCF + HF.$$

The RRKM rate constants determined by Holmes et al. [47] were used in the calculation (inverse Laplace transform version of the rate constants), and the parameters are listed in table 3. The vibrational frequencies of 1,1,2-trifluoroethane were taken from the recent assignment of the spectrum [48]. The assumed Lennard-Jones collision parameters, and optical absorption parameters are also listed in table 1 and the α parameters are in table 2

For the purposes of this paper, a laser fluence (at 1083.5 cm^{-1}) of 3.0 J cm^2 was assumed for an exponentially decaying pulse ($\tau = 1.0$ μs) and the argon pressure was varied. The fractional yields calculated for all three reaction channels as functions of collision frequency are presented in fig 11. For *efficient* colliders, we expect decomposition to occur at a rate competitive with collision frequency; for inefficient colliders, several collisions are necessary for deactivation and the unimolecular decomposition rate will be slower than the collision rate. In these calculations, most molecules decomposed at an energy of $\approx$ 32000–35000 cm^{-1}, corresponding to a decomposition rate constant of $\approx (1\text{–}5) \times 10^7$ s^{-1}, about a factor of 2–10 slower than the collision rate corresponding to 50% total reaction yield. The net optical pumping rate ($C_i^a - C_i^e$) at $E = 34000$ cm^{-1} is $\approx 5 \times 10^7$ s^{-1}, i.e. about the same as the decomposition rate

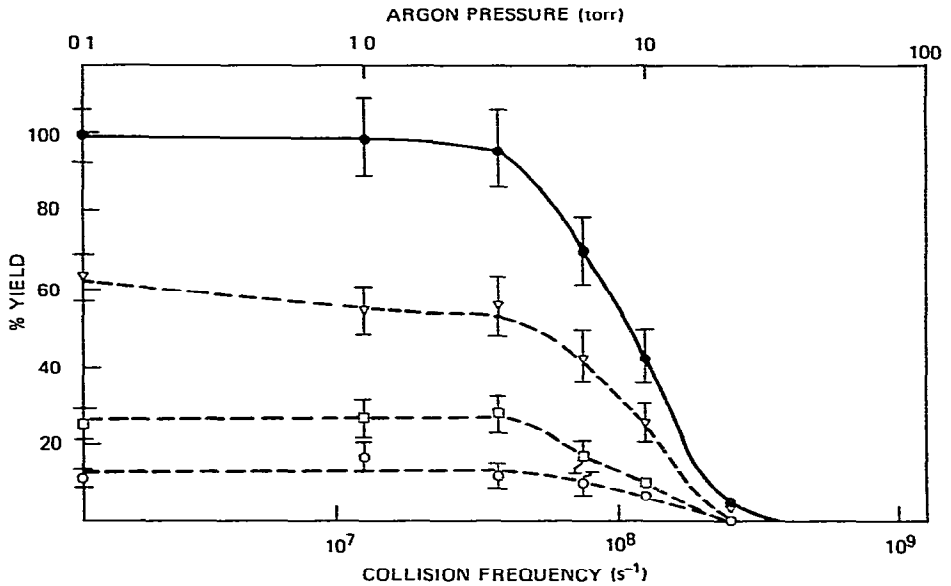

Fig 11. Yields versus collision frequency for a multiple-channel reaction system brought about by IR multiphoton decomposition ○ reaction (f), ▽ reaction (g), □ reaction (h), ● total reaction

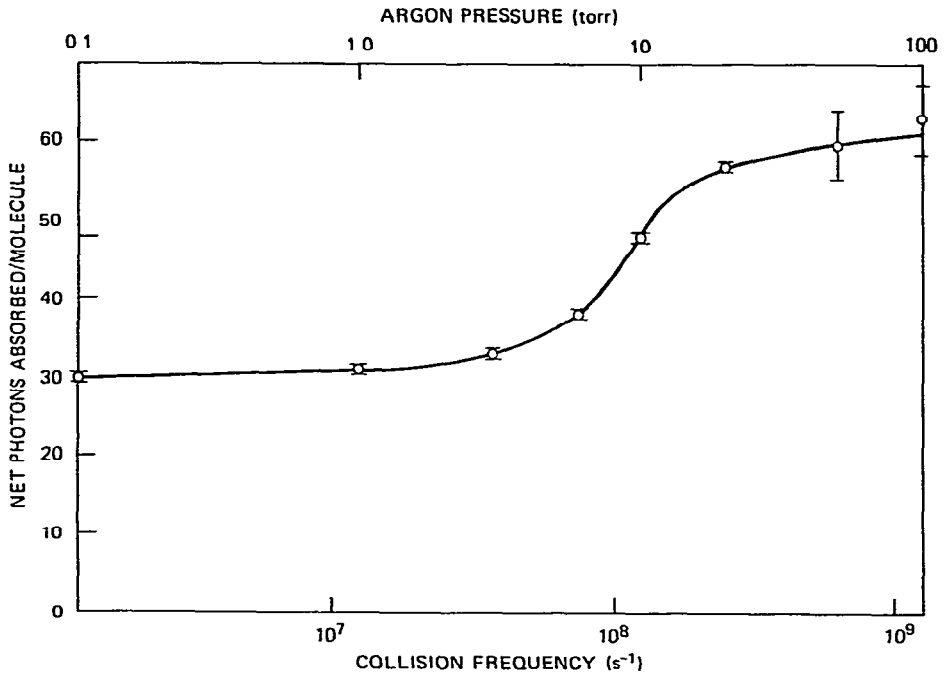

Fig 12 Net number of photons absorbed per molecule as a function of total pressure (constant laser fluence)

constant, as expected [24].

The average number of photons absorbed was also calculated and the results are presented in fig. 12. For low reaction yields (high pressures), each molecule can absorb photons, be collisionally deactivated, and then absorb more photons, repeatedly, without decomposing. This cyclic process explains the large number of photons absorbed at higher pressures. At low pressures, the photon-absorption–deactivation cycle is broken when the molecules decompose, resulting in fewer photons absorbed.

Although not presented here, the calculations also result in temporal histories of IRF, collider bath temperature, and population distributions, as described above for other examples. See ref. [49] for examples of collision-free multiphoton decomposition. Depending upon the experimental conditions, it is possible to investigate energy transfer, decomposition or optical absorption with little mutual interference. Thus, multiple photon absorption is potentially a very powerful experimental tool.

9.5. *Computational speed*

Monte Carlo techniques are somewhat time-consuming because random numbers must be generated for selection of variables and for every step of the stochastic trajectories. For simulations involving high collision frequencies, the length of machine-time required is directly proportional to the simulated time interval and to the collision frequency, i.e. the number of collisions.

For a typical "high-pressure" case, corresponding to 1 Torr of N_2 and 1 μs time duration, a single trajectory requires $\approx$ 10 s on our DEC LSI 11/02 laboratory computer. Simulations of collision-free experiments require less than 0.3 s of machine-time per trajectory for simulations of $\approx$ 1 μs duration.

10. Conclusions

The preceding examples show the utility of Monte Carlo techniques for solving a number of calculational problems of interest to kineticists. The computer code employed incorporates all of the features described, and is used in our laboratories to perform computations on chemical activation, on multiple photon absorption and decomposition, and on energy transfer. As noted earlier, the Monte Carlo approach is not efficient for "rare events", such as thermal decomposition reactions. On the other hand, the Monte Carlo technique makes feasible calculations on multiple photon absorption systems, which also include weak collisions – computations that would ordinarily require very large computers.

Acknowledgement

I am grateful for all of the many conversations with my co-workers and colleagues here at SRI and elsewhere. In particular, I wish to thank A.C. Baldwin, M.J. Rossi, G.P. Smith, D.M. Golden, R. Patrick, J.R. Pladziewicz, and R.J. Gordon, who were my co-workers on some of the papers referenced in the text.

References

[1] D C Tardy and B S Rabinovitch Chem Rev 77 (1977) 369
[2] M Quack and J. Troe, Gas Kinetics and Energy Transfer, Specialists Periodical Reports Vol. 2 (Chem Soc London 1977) p 175.
[3] P.A Schultz, Aa S Subdo, D J. Krajnovich H S Kwok, Y R Shen and Y.T. Lee, Ann Rev Phys Chem 30 (1979) 379
[4] D.M Golden, M J Rossi A C Baldwin and J R Barker, Accounts Chem Res 14 (1981) 56
[5] J F. Durana and J D McDonald, J. Chem Phys 64 (1976) 2518.
[6] S L Baughcum and S R Leone, J Chem Phys 72 (1980) 6531
[7] J R Barker and T Rothem Chem Phys 68 (1982) 331.
P L Trevor, T. Rothem and J R Barker, Chem Phys 68 (1982) 341
[8] G P Smith and J R Barker Chem. Phys Letters 78 (1981) 253
[9] M J Rossi and J R Barker Chem Phys Letters 85 (1982) 21.
[10] J R Barker M J. Rossi and J.R Pladziewicz, Chem Phys Letters 90 (1982) 99
[11] M.J Rossi J R Pladziewicz and J.R Barker, J. Chem Phys to be published
[12] H Hippler J. Troe and J J Wendelkin Chem Phys Letters 84 (1981) 257 J. Chem Phys., to be published
[13] K Luther and W Wieters Ber Bunsenges Physik Chem 85 (1981) 516
[14] K V Reddy and J M Berry, Faraday Discussions Chem Soc 67 (1979) 188 and references therein
[15] B D Cannon and F F Crim J Chem Phys 75 (1981) 1752
[16] D J Nesbitt and S R Leone, Chem Phys Letters 87 (1982) 123
[17] I Oref and B S Rabinovitch Accounts Chem 12 (1979) 166
[18] D.T. Gillespie J Comput Phys 22 (1976) 403, J Phys 81 (1977) 2340, J Comput Phys 28 (1978) 395
[19] J R Barker, J Chem Phys 72 (1980) 3686
[20] J O Hirschfelder, C F Curtiss and R B. Bird Molecular theory of gases and liquids (Wiley, New York, 1964)
[21] J. Troe J. Chem Phys 66 (1977) 4758
[22] J Troe, Ber Bunsenges Physik Chem 77 (1973) 665
[23] R G. Gilbert and K D King Chem Phys 49 (1980) 367.
[24] A C. Baldwin and J R Barker, J. Chem Phys 74 (1981) 3813, 3823, Chem Phys Letters 86 (1982) 55
[25] J C Stephenson D S King M F Goodman and J. Stone, J Chem Phys 70 (1979) 4496
[26] M Quack Ber Bunsenges Physik Chem 85 (1981) 318
[27] P J Robinson and K A Holbrook Unimolecular reactions (Wiley–Interscience, New York, 1972)
[28] W. Forst, Theory of unimolecular reactions (Academic Press, New York 1973)
[29] W. Forst J. Phys Chem 86 (1982) 1771, and references cited therein
[30] M Quack and J Troe, Ber Bunsenges Physik Chem 79 (1975) 170.
M Quack Nuovo Cimento 63 (1981) 358
[31] D Bunker and M Pattengill, J. Chem Phys 48 (1968) 772
[32] A J Stace Mol Phys 38 (1979) 155.
A J Stace and P V Sellers Chem Phys 50 (1980) 147.
[33] L Holmlid and K Rynefors, Chem. Phys 60 (1981) 393; K Rynefors and L Holmlid, Chem Phys 60 (1981) 405.
[34] G Herzberg, Infrared and Raman spectra (Van Nostrand Princeton 1945)
[35] G. Kohlmaier and B S Rabinovitch, J Chem Phys 38 (1963) 1692
[36] S P. Sander, M Peterson R T. Watson and R Patrick J Phys Chem 86 (1982) 1236
[37] R Patrick Ph D Thesis, Oxford University (1981)
[38] R Patrick and M.J Pilling Chem Phys. Letters 91 (1982) 343.
[39] R Patrick, M J. Pilling and G J Rogers Chem Phys 53 (1980) 279.

[40] R Patrick, J R. Barker and D M. Golden, J. Phys Chem., to be published
[41] J E Dove and J. Troe, Chem Phys 35 (1978) 1
[42] K D. King, D M. Golden, G.N Spokes and S W. Benson, Intern J Chem Kinetics 3 (1971) 411
[43] I E Klein and B S Rabinovitch, Chem Phys 35 (1978) 439,
K D King, T.T. Nguyen and R.G Gilbert, Chem Phys 61 (1981) 221.
[44] W D Lawrence, A E.W Knight, R.G Gilbert and K D. King, Chem Phys 56 (1981) 343
[45] A.C. Baldwin and H van den Bergh, J. Chem. Phys 74 (1981) 1012
[46] J E. Eberhardt, R.B Knott, A W. Pryor and R G. Gilbert, Chem Phys 69 (1982) 45
[47] B E Holmes, D W. Setser and G O Pritchard, Intern J Chem Kinetics, 8 (1976) 215.
[48] V F Kalasinsky, H V Anjana and T S Little, J Phys Chem 86 (1982) 1351.
[49] R E. Weston, J. Phys Chem 86 (1982) 4864.